Modulation instability in the weak dispersion regime of a dispersion modulated passive fiber-ring cavity

François Copie, Matteo Conforti, Alexandre Kudlinski, Stefano Trillo, Arnaud Mussot

Research Article | Vol. 25, No. 10 | 15 May 2017 | OPTICS EXPRESS 11283

Optics EXPRESS

Modulation instability in the weak dispersion regime of a dispersion modulated passive fiber-ring cavity

FRANÇOIS COPIE,[1,*] MATTEO CONFORTI,[1] ALEXANDRE KUDLINSKI,[1] STEFANO TRILLO,[2] AND ARNAUD MUSSOT,[1]

[1] *Univ. Lille, CNRS, UMR 8523-PhLAM-Physique des Lasers Atomes et Molécules, F-59000 Lille, France*
[2] *Department of Engineering, University of Ferrara, Via Saragat 1, 44122 Ferrara, Italy*
[*] *francois.copie@univ-lille1.fr*

Abstract: We present a theoretical and experimental study of the modulation instability process in a dispersion oscillating passive fiber-ring resonator in the low dispersion region. Generally, the modulation of the dispersion along the cavity length is responsible for the emergence of a regime characterised by multiple parametric resonances (or Faraday instabilities). We show that, under weak dispersion conditions, a huge number of Faraday sidebands can grow under the influence of fourth order dispersion. We specifically designed a piecewise uniform fiber-ring cavity and report on experiments that confirm our theoretical predictions. We recorded the dynamics of this system revealing strong interactions between the different sidebands in agreement with numerical simulations.

OCIS codes: (190.4370) Nonlinear optics, fibers; (190.3100) Instabilities and chaos; (230.5750) Resonators

References and links

1. R. Vallée, "Temporal instabilities in the output of an all-fiber ring cavity," Opt. Commun. **81**, 419–426 (1991).
2. M. Nakazawa, K. Suzuki, and H. A. Haus, "Modulational instability oscillation in nonlinear dispersive ring cavity," Phys. Rev. A **38**, 5193–5196 (1988).
3. M. Haelterman, S. Trillo, and S. Wabnitz, "Dissipative modulation instability in a nonlinear dispersive ring cavity," Opt. Commun. **91**, 401–407 (1992).
4. S. Coen and M. Haelterman, "Continuous-wave ultrahigh-repetition-rate pulse-train generation through modulational instability in a passive fiber cavity," Opt. Lett. **26**, 39–41 (2001).
5. G.-L. Oppo, "Formation and control of Turing patterns and phase fronts in photonics and chemistry," J. Math. Chem. **45**, 95 (2008).
6. R. Vallée, "Role of the group velocity dispersion in the onset of instabilities in a nonlinear ring cavity," Opt. Commun. **93**, 389–399 (1992).
7. S. Coen and M. Haelterman, "Modulational Instability Induced by Cavity Boundary Conditions in a Normally Dispersive Optical Fiber," Phys. Rev. Lett. **79**, 4139–4142 (1997).
8. S. B. Cavalcanti, J. C. Cressoni, H. R. da Cruz, and A. S. Gouveia-Neto, "Modulation instability in the region of minimum group-velocity dispersion of single-mode optical fibers via an extended nonlinear Schrödinger equation," Phys. Rev. A **43**, 6162–6165 (1991).
9. J. D. Harvey, R. Leonhardt, S. Coen, G. K. L. Wong, J. C. Knight, W. J. Wadsworth, and P. St.J. Russell, "Scalar modulation instability in the normal dispersion regime by use of a photonic crystal fiber," Opt. Lett. **28**, 2225–2227 (2003).
10. S. Pitois and G. Millot, "Experimental observation of a new modulational instability spectral window induced by fourth-order dispersion in a normally dispersive single-mode optical fiber," Opt. Commun. **226**, 415–422 (2003).
11. M. Droques, A. Kudlinski, G. Bouwmans, G. Martinelli, A. Mussot, A. Armaroli, and F. Biancalana, "Fourth-order dispersion mediated modulation instability in dispersion oscillating fibers," Opt. Lett. **38**, 3464–3467 (2013).
12. A. Armaroli and F. Biancalana, "Suppression and splitting of modulational instability sidebands in periodically tapered optical fibers because of fourth-order dispersion," Opt. Lett. **39**, 4804–4807 (2014).
13. A. Mussot, E. Louvergneaux, N. Akhmediev, F. Reynaud, L. Delage, and M. Taki, "Optical Fiber Systems Are Convectively Unstable," Phys. Rev. Lett. **101**, 113904 (2008).
14. F. Leo, A. Mussot, P. Kockaert, P. Emplit, M. Haelterman, and M. Taki, "Nonlinear Symmetry Breaking Induced by Third-Order Dispersion in Optical Fiber Cavities," Phys. Rev. Lett. **110**, 104103 (2013).
15. Y. Xu and S. Coen, "Experimental observation of the spontaneous breaking of the time-reversal symmetry in a synchronously pumped passive Kerr resonator," Opt. Lett. **39**, 3492 (2014).

#291441 https://doi.org/10.1364/OE.25.011283
Journal © 2017 Received 29 Mar 2017; accepted 1 May 2017; published 4 May 2017

Optics EXPRESS

16. P. Parra-Rivas, D. Gomila, F. Leo, S. Coen, and L. Gelens, "Third-order chromatic dispersion stabilizes Kerr frequency combs," Optics Letters **39**, 2971 (2014).
17. M. Tlidi, A. Mussot, E. Louvergneaux, G. Kozyreff, A. G. Vladimirov, and M. Taki, "Control and removal of modulational instabilities in low-dispersion photonic crystal fiber cavities," Opt. Lett. **32**, 662–664 (2007).
18. M. Conforti, A. Mussot, A. Kudlinski, and S. Trillo, "Modulational instability in dispersion oscillating fiber ring cavities," Opt. Lett. **39**, 4200–4203 (2014).
19. M. Conforti, F. Copie, A. Mussot, A. Kudlinski, and S. Trillo, "Parametric instabilities in modulated fiber ring cavities," Opt. Lett. **41**, 5027–5030 (2016).
20. F. Copie, M. Conforti, A. Kudlinski, A. Mussot, and S. Trillo, "Competing Turing and Faraday Instabilities in Longitudinally Modulated Passive Resonators," Phys. Rev. Lett. **116**, 143901 (2016).
21. F. Copie, M. Conforti, A. Kudlinski, S. Trillo, and A. Mussot, "Dynamics of Turing and Faraday instabilities in a longitudinally modulated fiber-ring cavity," Opt. Lett. **42**, 435 (2017).
22. N. Tarasov, A. M. Perego, D. V. Churkin, K. Staliunas, and S. K. Turitsyn, "Mode-locking via dissipative Faraday instability," Nat. Commun. **7**, 12441 (2016).
23. L. A. Lugiato and R. Lefever, "Spatial Dissipative Structures in Passive Optical Systems," Phys. Rev. Lett. **58**, 2209–2211 (1987).
24. S. Coen, M. Haelterman, P. Emplit, L. Delage, L. M. Simohamed, and F. Reynaud, "Bistable switching induced by modulational instability in a normally dispersive all-fibre ring cavity," J. Opt. B: Quantum Semiclass. Opt. **1**, 36 (1999).
25. D. R. Solli, G. Herink, B. Jalali, and C. Ropers, "Fluctuations and correlations in modulation instability," Nat. Photonics **6**, 463–468 (2012).
26. B. Wetzel, A. Stefani, L. Larger, P. A. Lacourt, J. M. Merolla, T. Sylvestre, A. Kudlinski, A. Mussot, G. Genty, F. Dias, and J. M. Dudley, "Real-time full bandwidth measurement of spectral noise in supercontinuum generation," Sci. Rep. **2**, 882 (2012).
27. S.-W. Huang, "Multispectral Kerr frequency comb initiated by Faraday ripples," https://arxiv.org/abs/1610.06657 (2016).

1. Introduction

Nonlinear fiber cavities have been widely studied during the last 30 years. The inclusion of fibers' Kerr nonlinearity in a passive system subject to optical feedback opens the way to a large variety of instabilities [1] among which modulation instability (MI) plays a significant role [2,3]. Arising from the interplay between losses and driving on one side and nonlinearity and dispersion on the other side, MI in nonlinear cavities has attracted a lot of attention as it allows the generation of ultra-fast train of pulses from a continuous or quasi-continuous wave excitation [4]. In this context MI is usually referred to as Turing instability by analogy with the mechanism of pattern formation in the context of chemical reactions [5].

The group velocity dispersion (GVD) is one of the most important parameters of the cavity [6]. To date, most studies of intracavity MI have addressed the case of rather large group velocity dispersion in both the anomalous [2, 4] and normal [7] regimes. In these cases, it is legitimate to take into account only the second order dispersion term β_2, but when investigating MI under weak dispersion the impact of higher order dispersion (HOD) becomes significant. Indeed, it is well known that in fibers (in the single-pass configuration) with small β_2, the MI process is affected by HOD terms. For example, the fourth order dispersion (FOD, β_4) can extend the range of existence of MI to the normal dispersion regime [8–10]. In periodic dispersion fibers the impact of β_4 is also significant. Indeed, it can either produce new sidebands in the spectrum [11] or suppress the MI process [12]. HOD terms have been found to be at the origin of numerous effects in cavities as well. Recent studies have shown, for example, that the first HOD term (β_3) is responsible for the emergence of convective and absolute instabilities [13], the asymmetry observed in intracavity MI spectrum [14] or short pulses spectrum [15]. β_3 also impacts the stability of Kerr frequency combs triggered by MI in both fiber cavities and microresonators [16]. It was also predicted that the FOD might give rise to a new unstable frequency in low dispersion photonic crystal fiber cavities [17].

In previous works we found that a longitudinal step-like dispersion profile along the length of the cavity gives rise to a new regime of instability originating from parametric resonance that we refer to as Faraday regime, which coexists with the well established Turing regime [18–21].

Optics EXPRESS

Such a Faraday mechanism is attracting a lot of attention as a general mechanism related to parametric driving in fiber cavities [22]. In our passive cavity, the Faraday regime of instability results in high frequency parametric sidebands in the optical spectrum. In the first experimental investigations of this kind of resonator, composed of two sections of fibers spliced together, the local dispersion encountered by light was rather high so that the impact of HOD was not significant [20, 21].

In this work, we study a dispersion modulated fiber-ring cavity pumped close to the zero-dispersion wavelength (ZDW) of one fiber section. As a consequence, a huge number, up to 125, of quasi-phase-matched Faraday sidebands are observed at the output of the cavity thanks to the contribution of FOD. The paper is organized as follows: in Section 2 we extend our previous model [18] to higher order dispersion terms. We especially show that β_4 drastically changes the shape of the parametric gain spectrum when the cavity is pumped in the vicinity of a ZDW with the formation of high frequency sideband clusters. In Section 3 we report on the experimental observation of such spectra in excellent agreement with theoretical predictions. The round-trip-to-round-trip evolution of the instability spectrum is also investigated and features strong multiple wave mixing leading to a stationary regime in agreement with numerical simulations. Conclusions are drown in Section 4 and some perspectives are given.

2. Theory

In passive fiber-ring cavities with a step-like GVD profile an additional regime of parametric instability appears, that we called *Faraday regime* [18, 20, 21] in addition to the well-known *Turing regime*. This latter can be fully interpreted by considering average parameters of the cavity contrary to the *Faraday regime* which only exists thanks to the modulated GVD [18–20]. In the previous experiments, the values of dispersion of each fiber were relatively high and thus the behaviour of the system was dominated by the second order dispersion β_2.

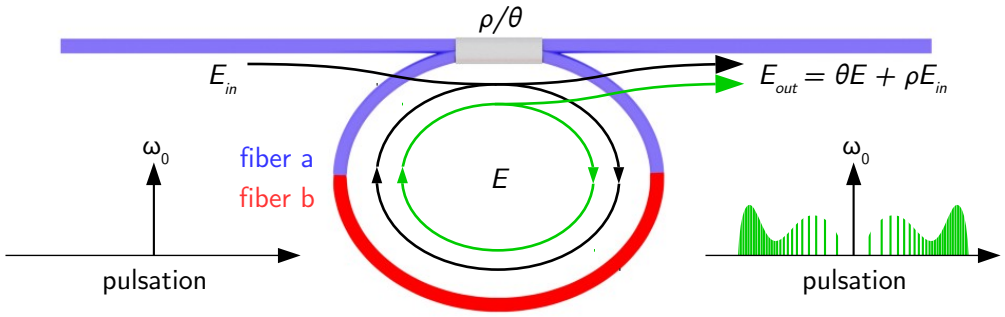

Fig. 1. Schematic representation of a dispersion modulated passive fiber-ring cavity. A monochromatic pump (at pulsation ω_0) drives a loop composed of two fibers with different dispersion (represented in blue and red). The output field is composed of a superposition of the input and intracavity field in proportions governed by the reflection and transmission coefficients of the coupler (ρ and θ respectively, $\rho^2 + \theta^2 = 1$).

In this section, we extend the previous theoretical model to higher order dispersion terms which become significant in regions of low dispersion. To do so, we consider the following generalized mean field Lugiato-Lefever (LL) equation [3, 23] which describes light propagation inside the ring cavity:

Optics EXPRESS

$$i\frac{\partial E(z,t)}{\partial z}+\sum_{q=2}^{N}\frac{i^q\beta_q(z)}{q!}\frac{\partial^q E(z,t)}{\partial t^q}+\gamma|E(z,t)|^2E(z,t)=\left(\frac{\delta}{L}-i\frac{\alpha}{L}\right)E(z,t)+i\sqrt{\theta}E_{in}, \quad (1)$$

where $E(z,t)$ is the intracavity electric field envelope , z measures the distance and t is the time in the frame travelling at the group velocity of the pump. γ is the nonlinear coefficient, $\beta_q(z)$ the longitudinal profile of the dispersion of order q along the ring of length L. α accounts for the losses related to the finesse of the cavity by $\alpha \approx \pi/F$, δ the cavity detuning and E_{in} the input field driving the cavity. θ is the transmission coefficient defined such that $\theta^2+\rho^2=1$. Also, it is customary to introduce the normalized detuning $\Delta=\delta/\alpha$ [3,20,21,24].

We perform the stability analysis of this equation relative to the ansatz $E(z,t)=\sqrt{P_u}+(u(z,t)+iv(z,t))$, where P_u is the intracavity power and u, v are small real perturbations. By introducing the Fourier transform in time [$\tilde{u}=\int u\exp(i\omega t)dt$ and $\tilde{v}=\int v\exp(i\omega t)dt$], the linearised problem reduces to the following set of coupled linear differential equations:

$$\frac{\partial}{\partial z}\begin{bmatrix}\tilde{u}\\ \tilde{v}\end{bmatrix}=\begin{bmatrix}-(\alpha+i\zeta) & -g(z)\\ h(z) & -(\alpha+i\zeta)\end{bmatrix}\begin{bmatrix}\tilde{u}\\ \tilde{v}\end{bmatrix}, \quad (2)$$

with

$$\begin{cases}\zeta=\sum\limits_{q=2}^{\infty}i\beta_{2q-1}(z)(2q-1)!\omega^{2q-1},\\ g(z)=\sum\limits_{q=1}^{\infty}i\beta_{2q}(z)(2q)!\omega^{2q}+\gamma P_u-\delta L,\\ h(z)=\sum\limits_{q=1}^{\infty}i\beta_{2q}(z)(2q)!\omega^{2q}+3\gamma P_u-\delta L\end{cases} \quad (3)$$

Starting from Eqs. (2) and (3), we follow the same approach discussed in detail in the supplemental of Ref. [20] . We consider a ring cavity composed of two different pieces of uniform fiber labelled *fiber a* and *fiber b* in Fig. 1 and we limit the expansion up to the fourth order dispersion term β_4 (i.e., $N=4$ in Eq. (1)) since higher orders do not significantly impact the behaviour of the system. Under the assumption that losses and odd order dispersion terms do not vary inside the cavity, the following *parametric resonance* conditions are derived:

$$\left(\frac{\beta_2^{av}\omega^2}{2}+\frac{\beta_4^{av}\omega^4}{24}+2\gamma P_u-\delta\right)^2-\gamma^2P_u^2=\left(\frac{m\pi}{L}\right)^2, \quad (4)$$

where $\beta_{2,4}^{av}$ are the average second and fourth order dispersion terms over the cavity length and m is an integer. It is then straightforward to find that these conditions are fulfilled for angular frequencies:

$$\omega_m=\pm\sqrt{-6\frac{\beta_2^{av}}{\beta_4^{av}}\pm2\sqrt{9\left(\frac{\beta_2^{av}}{\beta_4^{av}}\right)^2+\frac{6}{\beta_4^{av}}\left\{\pm\sqrt{\left(\frac{m\pi}{L}\right)^2+\gamma^2P_u^2}+\left(\frac{\delta}{L}-2\gamma P_u\right)\right\}}}. \quad (5)$$

From this equation it appears that an infinite number of resonances exists each one related to an order m. The parametric gain $G(\omega)$ can be calculated according to the following set of expressions:

Optics EXPRESS

$$\begin{cases} G(\omega) = \ln(\max|\sigma^{\pm}|)/L, \\ \sigma^{\pm} = D2 \pm \sqrt{D^2 4 - e^{-2\zeta L}} \\ D = e^{-\zeta L}\left[2\cos(k_a L_a)\cos(k_b L_b) - g_a h_b, + g_b h_a k_a k_b \sin(k_a L_a)\sin(k_b L_b)\right], \\ k_{a,b} = \sqrt{g_{a,b} h_{a,b}}, \end{cases} \tag{6}$$

where a (b) refers to the *fiber a* (b).

At this point, we recall the expression of the frequencies of the MI sidelobes in cavities with modulated dispersion without the contribution of β_4 [18]:

$$\omega_m = \sqrt{\left\{\frac{2}{\beta_2^{av}}\left(\frac{\delta}{L} - 2\gamma P_u\right)\right\} \pm \left[\frac{2}{\beta_2^{av}}\sqrt{\left(\frac{m\pi}{L}\right)^2 + (\gamma P_u)^2}\right]}, \tag{7}$$

and in the well-known case of uniform cavities [3]:

$$\omega = \sqrt{\frac{2}{\beta_2^{av}}\left(\frac{\delta}{L} - 2\gamma P_u\right)}, \tag{8}$$

that will be useful in the next sections.

We computed the parametric gain from Eq. (6) for a cavity composed of two uniform fibers of equal length (i. e. $L_a = L_b = L/2$). We consider the system to be in the bistable regime ($\Delta = 4$ [3]) with steady state set on the upper branch of the cavity response as illustrated in Fig. 2(b) ($P_u = 7.8\ W$). For uniform cavities, this branch is modulationally unstable in the average anomalous dispersion regime with the characteristic frequency of Eq. (8) and stable in the average normal dispersion regime [3].

Let us first consider the case $\beta_4 = 0$ (Fig. 2). The evolution of the GVD of each fiber composing the cavity is represented in Fig. 2(a) as a function of the wavelength and shows each fiber zero dispersion wavelength (ZDW) λ_0^a and λ_0^b respectively. The average dispersion of the cavity is plotted in black and lies in between the two previous curves and the resulting average zero dispersion wavelength is $\lambda_0^{av} = (\lambda_0^a + \lambda_0^b)/2$. Figure 2(c) displays a 2D color plot of the parametric gain spectrum (y axis) as a function of the pump wavelength (x axis) calculated from Eqs. (6). For $\lambda_P << \lambda_0^a$ the average dispersion is normal and the spectrum exhibits only two weak sidebands. When increasing the wavelength the number of bands grows, is maximum for $\lambda_P = \lambda_0^a$, and then decreases until no sidebands exists in the vicinity of λ_0^{av}. The position of each sideband corresponds to a solution of Eq. (7) for $m \neq 0$. For example, the calculated position for the $m = 1$ condition is superimposed (see dashed gray lines). For longer wavelengths the average dispersion becomes anomalous. Again, several pairs of sidebands emerge and when $\lambda_P = \lambda_0^b$ a large number of bands appear in a fashion similar to the case $\lambda_P = \lambda_0^a$. Then, less and less sidebands exist as the wavelength is further increased above λ_0^b. The main difference between the average normal and average anomalous region is the pair of broad, low frequency and high gain bands that can be seen in the anomalous regime. These bands are associated to the well-known MI in the anomalous dispersion region of uniform cavities [3] as it can be inferred from the agreement with the predictions of Eq.(8) (superimposed in dashed green lines) which gives the position of the MI sidelobes in the case of constant dispersion.

In order to get a clearer insight of what occurs when λ_P lies in the vicinity of one of the ZDW of the cavity, a closer view of the region around λ_0^a (rotated by 90 degrees anticlockwise for convenience) is plotted in Fig. 2(d). The gain spectrum exhibits more and more sidebands as λ_P approaches λ_0^a as highlighted in Figs. 2(e-g) which show three specific spectra. For $\lambda_P = \lambda_0^a$, an infinite number of sidebands are destabilized with almost the same gain (Fig. 3(e)).

This latter observation results from the exact cancellation of the dispersion operator for that specific pump wavelength and is thus not physically meaningful. Indeed, in regions of low

Optics EXPRESS

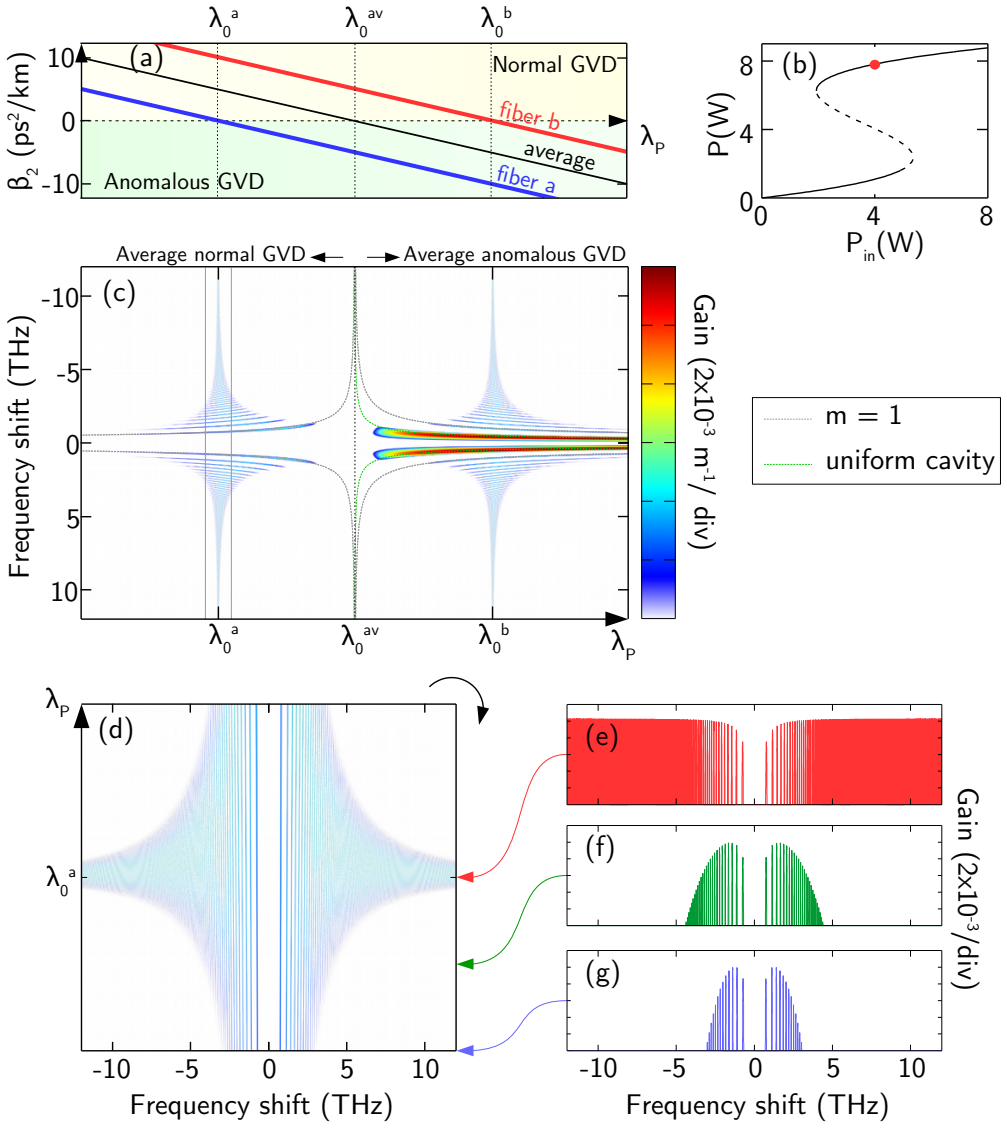

Fig. 2. MI in the Faraday regime with only GVD: (a) Evolution of the GVD as a function of the pump wavelength λ_P for the two fibers composing the ring. (b) Bistable response of the cavity, the operating point is marked by a red bullet. (c) 2D plot of the parametric gain spectrum as a function of the pump wavelength. The theoretical position of the first sidebands calculated from Eq. (7) in gray and Eq. (8) in green are superimposed. (d) Close-up view of (c) in the vicinity of λ_0^a (rotated by 90 degrees anticlockwise). (e-g) Parametric gain spectra for three pump wavelengths indicated by colored arrows in (d). $\beta_4 = 0\ s^4/m$, $L = 43\ m$.

dispersion (i. e. in the vicinity of a ZDW) HOD terms become significant and cannot be neglected anymore. This realistic configuration is represented in Fig. 3 which keeps the same structure as Fig. 2 except that we accounted for the FOD. In this exemple β_4 is negative as it is the case in most optical fibers, and constant all along the cavity length. Note that β_3 and more generally odd order dispersion terms do not play any role in the parametric gain. Figure 3(a) represent the

Optics EXPRESS

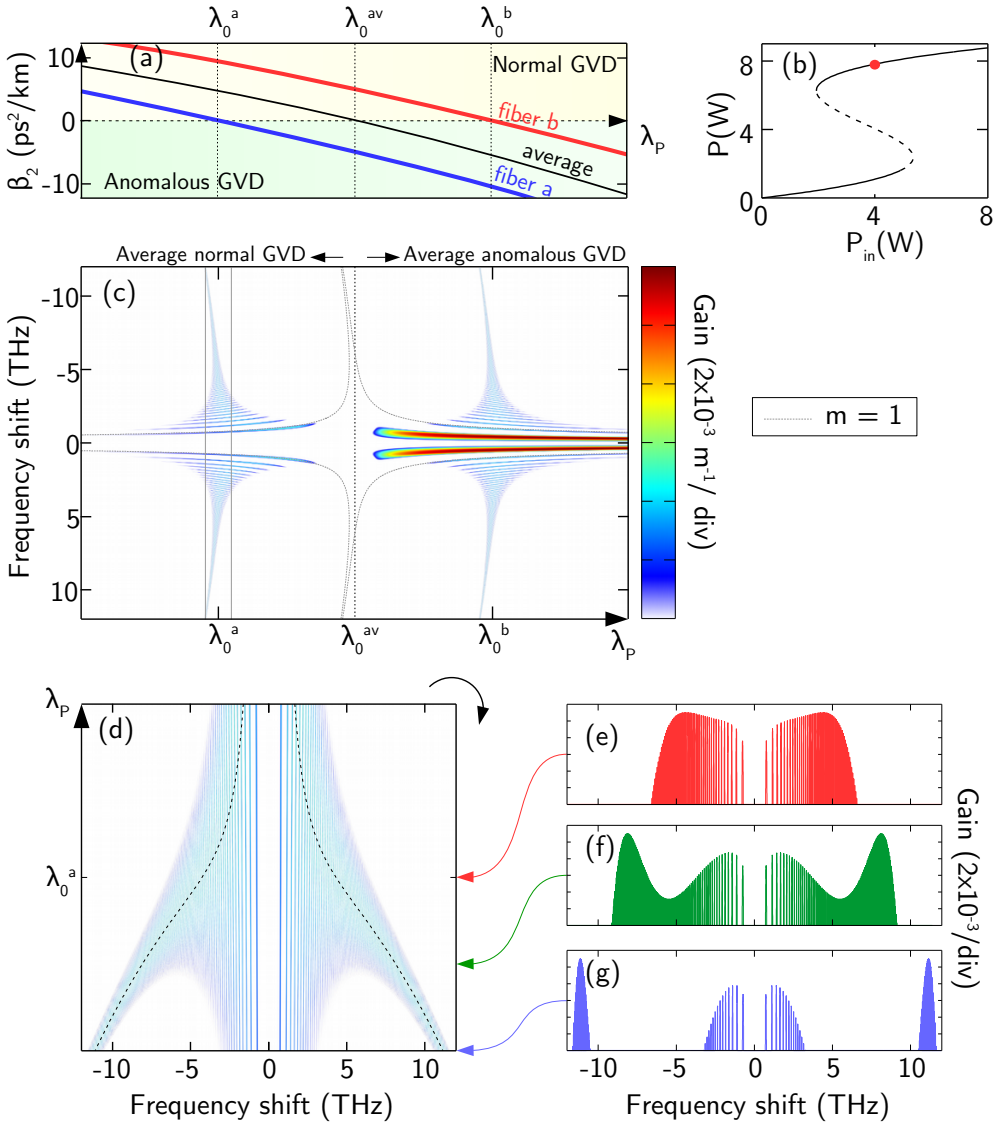

Fig. 3. MI in the Faraday regime when accounting for FOD: (a,b) as Fig. 2; (c) The theoretical position of the sidebands for $m = 1$ calculated from Eq. (5) is superimposed in gray. The position of the FOD branches calculated from Eq. (9) is highlighted by dashed black lines in (d). $\beta_4 = -10 \cdot 10^{-55}\ s^4/m$, $L = 43\ m$.

dispersion of each fiber as a function of the wavelength and Fig. 3(b) the bistable response of the cavity. It appears from Fig. 3(c) that the parametric gain spectrum is influenced by β_4 mostly in the vicinity of the ring's ZDWs (i. e. when the dispersion is locally low) and remains the same otherwise. It can also be pointed out that the predicted positions of the sidebands by Eq. (5) (in dashed grey lines) is essentially the same as when $\beta_4 = 0$. Fig. 3(d) shows a close-up view of the region around λ_0^a as in Fig. 2(d) and clearly illustrates the strong modification of the gain spectrum under the influence of β_4. Indeed, the branches that tend toward infinite frequencies in Fig. 2(d) are now curved toward lower wavelengths. At the ZDW of *fiber a* (λ_0^a) the gain spectrum is now limited to a rather narrow range of frequencies and the number of sidebands

Optics EXPRESS

becomes finite (Fig. 3(e)). For shorter pump wavelengths the gain spectrum is also significantly modified by the presence of β_4. Indeed, new higher frequency *clusters* of sidebands appear. For wavelength just slightly shorter than λ_0^a (Fig. 3(f)) these *clusters* are still connected to the lowest frequency sideband pairs (which are nearly unaffected by β_4) and form a rather broad spectrum. But for even shorter wavelengths (Fig. 3(g)) they eventually form detached high frequency *clusters* . Note that the same observation stands around the ZDW of *fiber b* (λ_0^b) in the average anomalous GVD region (see Fig. 3(c)).

The existence of the high frequency *clusters* is thus due to the FOD and their spectral positions can be calculated by noting that it is solely driven by the even dispersion coefficients (β_2 and β_4) of the locally low dispersion fiber section (*fiber a* in the case of Fig. 3(c-f)). It simply follows by dropping the contribution of the dispersion modulation in Eq. (5). This leads to the following expression for the position of the β_4 induced *clusters*:

$$\omega_{FOD} = \pm\sqrt{-6\frac{\beta_2^a}{\beta_4^a} \pm 2\sqrt{9\left(\frac{\beta_2^a}{\beta_4^a}\right)^2 + \frac{6}{\beta_4^a}\left(\frac{\delta}{L} - 2\gamma P_u\right)}}. \tag{9}$$

This frequency is reported in Fig. 3(d) in dashed black lines and coincide with the maximum of the envelope of the spectrum.

3. Experiments

3.1. Setup

We designed a ring cavity similar to the one depicted in Fig. 1. It is composed of 22.6 m of dispersion shifted fiber (DSF) with a ZDW at 1551.05 nm (*fiber a*) and 20.5 m of dispersion compensating fiber (DCF) (*fiber b*). The evolution of the GVD as a function of the wavelength is represented in Fig. 4(a) for the two fibers. The range of pump wavelengths accessible in the experiment is shaded and corresponds to a small region below λ_0^a. In this region, all the predicted sidebands exhibit a parametric gain of the same order of magnitude (see Fig. 3(d)) which facilitate their observation as opposed to the region around λ_0^b where the first pair of sidebands has a parametric gain six times larger than the others. Figures 4(b, c) display the evolution over three round-trips of β_2 and β_4 respectively. We can see that, for the range of pump wavelength investigated, both fibers exhibit normal dispersion with a nearly constant difference ($\approx 10\ ps^2/km$). Furthermore, *fiber a* exhibits a very low GVD in this region which will emphasize the effect of β_4. The two fibers are characterized by fourth order dispersions of respectively $\beta_4^a = -1 \times 10^{-3}\ ps^4/km$ and $\beta_4^b = 1.38 \times 10^{-3}\ ps^4/km$ ($\beta_4^{av} \approx 1.3 \times 10^{-4}\ ps^4/km$) and the nonlinearity is estimated to be $\gamma = 2.5\ /W/km$ for both fibers. We measured a finesse of 18 and thus $\alpha \approx 0.17$. For all the following experiments the detuning was fixed to $\pi/4.5\ rad$ which leads to a normalized detuning $\Delta = \delta/\alpha = 4 > \sqrt{3}$, that is to say the cavity was driven in the bistable regime [3]. It is worth noting that for this set of parameters, only the upper branch of the bistable cycle exhibits Faraday MI since the system cannot exhibit stable Turing patterns on the lower branch unless $\Delta > 4.25$ [24].

The setup used for the experiments is depicted in Fig. 5(a) and is similar to the one used in our previous studies ([20, 21]). A continuous wave laser with very low spectral width ($< 1\ kHz$) and tunable wavelength (between 1549.6 nm and 1550.3 nm) is chopped by an electro-optic modulator (EOM 1) to produce a train of 400 ps square pulses at a repetition rate of 4.74 MHz which corresponds to the round-trip time of the 43.14 m long cavity. Those pulses are amplified to peak powers up to a few watts thanks to an erbium doped fiber amplifier (EDFA) and the pump is filterd out by a narrow tunable band-pass filter (BPF) to remove amplified spontaneous emission (ASE) in excess. A second polarization dependant EOM (EOM 2) works as a variable attenuator to control the input pump power and is also used to tailor the train of pulses into periodic bursts (see Fig. 5(b)). Input pulses are directed to the input 90/10 coupler of the cavity through a

Optics EXPRESS

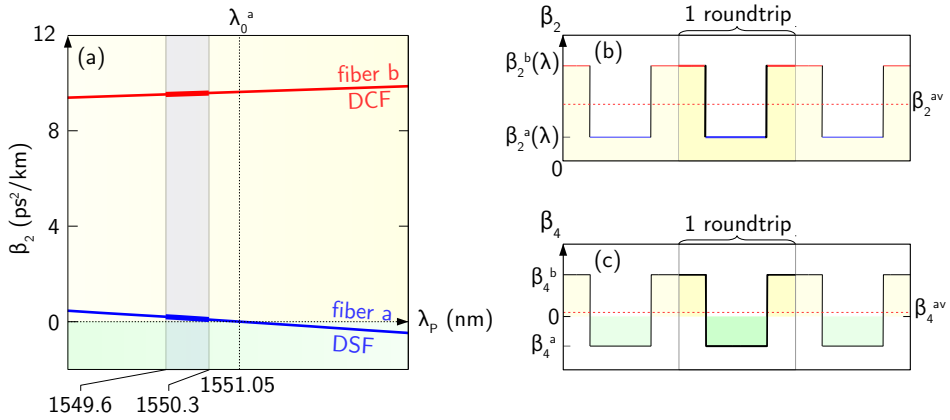

Fig. 4. (a) GVD as a function of the wavelength for the two fibers which constitute the ring cavity. The shaded region corresponds to the accessible range of pump wavelengths. Longitudinal profiles of (b) β_2 and (c) β_4 for three consecutive round-trips. The average values of β_2 and β_4 are represented in dashed red lines.

circulator which allows us to actively stabilise the cavity length against acousto-mechanical perturbation with a precision of the order of $\lambda_0/200$ using a counter propagating reference beam. The output of the cavity can be analysed simultaneously using two different detection schemes: (i) An optical spectrum analyser (OSA) displays the full spectrum averaged over thousands of round-trips typically with a resolution of 4 GHz; (ii) A setup based on the real-time dispersive Fourier transformation (rt-DFT) technique allows the recording of round-trip-to-round-trip spectra but offers a lower resolution (≈ 30 GHz) and dynamics [21].

A particular attention has to be paid to the driving intensity of the cavity. Indeed, the regime of instability we investigate is characterized by tens of spectral sidebands. It is important to emphasize here that the theoretical spectra shown so far in Fig. 2 and 3 are gain spectra which do not take into account wave mixing between the different MI gain bands. The consequence of such a potential parasitic wave mixing is that the output spectra when a steady state is reached is not likely to contain every predicted gain bands. It is thus necessary to circumvent this detrimental wave mixing to allow the recording of all the sidebands by means of an OSA. One way to do so is to reduce the power of the quasi-phase-matched (QPM) sidebands as it is known that the wave mixing is less effective when the power of the frequency components is low. To achieve this we propose a pumping technique that we labelled *short burst pumping* which is illustrated in Fig. 5(b). It consists of periodically turning on and off the coherent driving of the cavity so that the QPM sidebands do not reach a power level for which wave mixing is detrimental. When the driving field is on, the power of the sidebands grows (see the dashed red line in Fig. 5(b)) and when it is turned off, the power decays exponentially as the cavity empties itself. For comparison, the evolution of the signal power if the driving field is not turned off is sketched as a dashed black line. The *on* and *off* durations were adjusted experimentally: ΔT_1 is the largest value for which no evidence of spurious wave mixing is seen in the output spectrum, thus maximising the signal power while circumventing the wave mixing issue. The dead time ΔT_0 was set just long enough to ensure that each burst acts as an independent run of the experiment. It should be noted that it typically takes a few seconds to record an OSA trace which corresponds to thousands of consecutive bursts in our case. Such recordings are therefore average representations of the dynamics of the cavity at the early stage of the parametric amplification as it will be discussed in the last section.

Optics EXPRESS

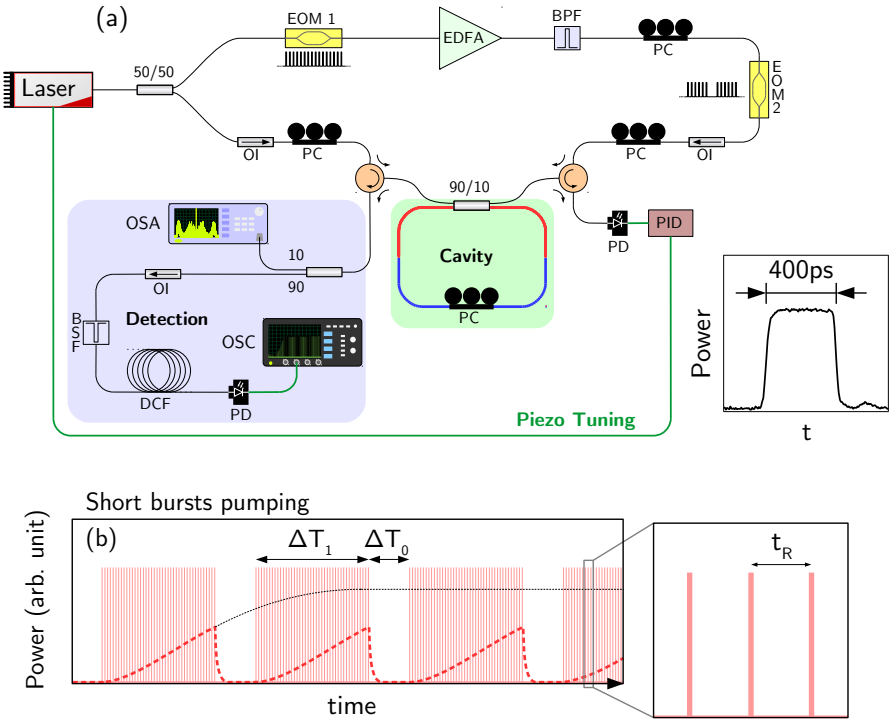

Fig. 5. (a) Experimental setup. (b) Schematic representation of the short bursts pumping method used in this work. The input pump pulses are in light red and a sketch of the corresponding signal power is represented by a dashed red line. The evolution of the signal power when the driving field is not turned off after the first burst is reported as a black curve for comparison. Inset of (b) displays a zoom over three consecutive round-trips.

3.2. *Observation of complex parametric instability spectra*

We applied the "*short bursts pumping*" method to observe a very large number of sidebands when the pump wavelength lies in the vicinity of the ZDW of one fiber (Figure 3(f) typically).

Firstly we confirm the dependence of the instability spectrum on the pump wavelength. Fig. 6(a) displays a 2D color plot of the experimental output spectrum for pump wavelengths varying from 1549.6 to 1550.3 nm, constant input peak power of 4 W and normalized detuning $\Delta = 4$. $\Delta T_1 = 100\ \mu s$ (475 pulses) and $\Delta T_0 = 10\ \mu s$. Under these conditions the system evolves on the higher transmission branch of the bistable cycle. As predicted by our theoretical study, multiple sideband pairs are observed with symmetric location around the pump, as shown in Fig. 6(a). In particular, clusters of narrow sidebands which position strongly depends on the pump wavelength appear at high frequency. As the pump wavelength is increased closer to the ZDW of *fiber a* (1551.05 nm), the clusters drift toward lower frequency until the spectrum exhibits a quasi-continuum of sidebands spanning more than 16 THz (130 nm) for $\lambda_P = 1550.3\ nm$. The position of the clusters is in excellent agreement with the predictions of Eq. (9) (superimposed in dashed black lines) which correspond to a uniform cavity with FOD. Figure 6(b) shows eight spectra picked along Fig. 6(a) in order to better appreciate these results, which qualitatively agree with the theoretical behaviour described in Fig. 3(d-g). The position of each pair of sidebands corresponds to a fulfilled parametric resonance condition (Eq. (4)). By noting that the frequency of the band grows with the value of the integer m (Eq. (5)), we can identify each peak up to the

Optics EXPRESS

order $m = 125$ in the spectrum at the bottom.

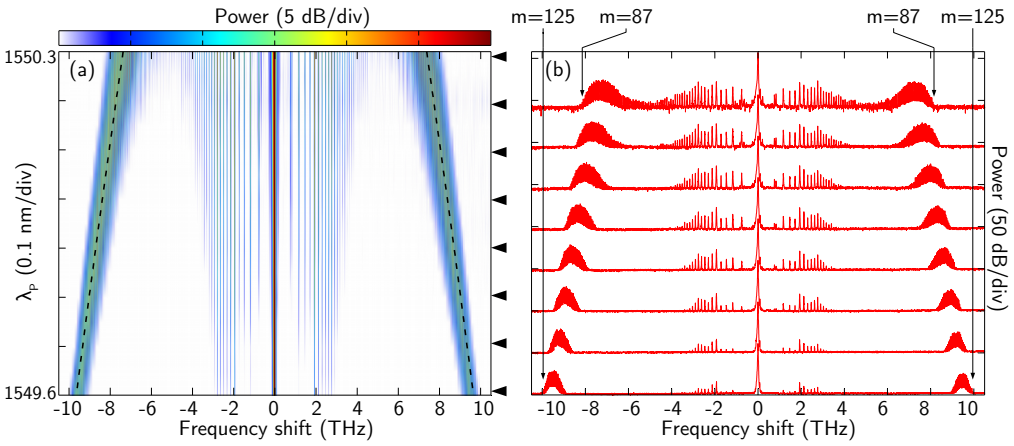

Fig. 6. (a) Experimental evolution of the output spectra of the cavity as a function of the pump wavelength. The analytical estimation (Eq. (9)) of the position of the *HOD branch* is in dashed black lines. Eight spectra along this figure (indicated by black triangles) are reported in (b) for clarity. The positions and orders of the high-frequency cut-off sidebands are highlighted by arrows for the first and last spectra.

A quantitative comparison between theory and experiments is displayed in Fig. 7 for the largest pump wavelength ($\lambda_P = 1550.3\ nm$) which is the one producing the largest number of sidebands in the spectrum. The experimental spectrum (Fig. 7(a)) shows a very strong resemblance in its shape with the analytical gain spectrum (Fig. 7(b)). Notice the reduced visibility of the bands in the clusters around $\pm 7\ THz$ in experiments that are likely due to the limited spectral resolution of the OSA ($4\ GHz$). Fig. 7(c) displays the position of each sideband as a function of its order m for both the experiment and the analytics. It highlights that the bands get closer to each other as m increases as expected from Eq. (5). As can be seen, a perfect agreement between theory and experiments is obtained for the positions of the 87 pairs of sidebands.

3.3. Competition between sidebands

As described before, parasitic wave mixing between the different parametric sidebands is expected to be increasingly significant as the power of the sidebands grow (and thus as the number of round-trips increases). This is why we limited the burst duration to 475 round-trips so far. To investigate the competition between the different sidebands we need to access the round-trip-to-round-trip dynamics of the spectrum which is not possible using an OSA due to its large recording time compared to the round-trip time of the cavity. We thus employ the DFT method described previously and in Ref. [21] to unveil the dynamical behaviour of our system. Indeed, this method allows us to record the spectrum of each pulse exiting the cavity. Then the dynamics of the spectrum is obtained by stacking the successive recordings. We use the same pumping method as before, though setting the duration of the bursts to $\Delta T_1 = 1.5\ ms$ (≈ 7000 pulses) to let the system reach a stationary state. We use a highly dispersive fiber, characterized by the following parameters: $\beta_2 L = 870\ ps^2$ and $\beta_3 L = -5.5\ ps^3$, to realise the frequency-to-time conversion. The spectrum is then retrieved from the time traces thanks to the mapping $T(f) = 2\pi^2\beta_3 L(f - f_0)^2 + 2\pi\beta_2 L(f - f_0)$, where $f_0 = c/\lambda_0$ is the optical frequency of the pump laser.

Figure 8(b) showcases the experimental evolution of the instability spectrum at the output of the cavity for 1500 consecutive round-trips after turning on the driving input field for the same

Optics EXPRESS

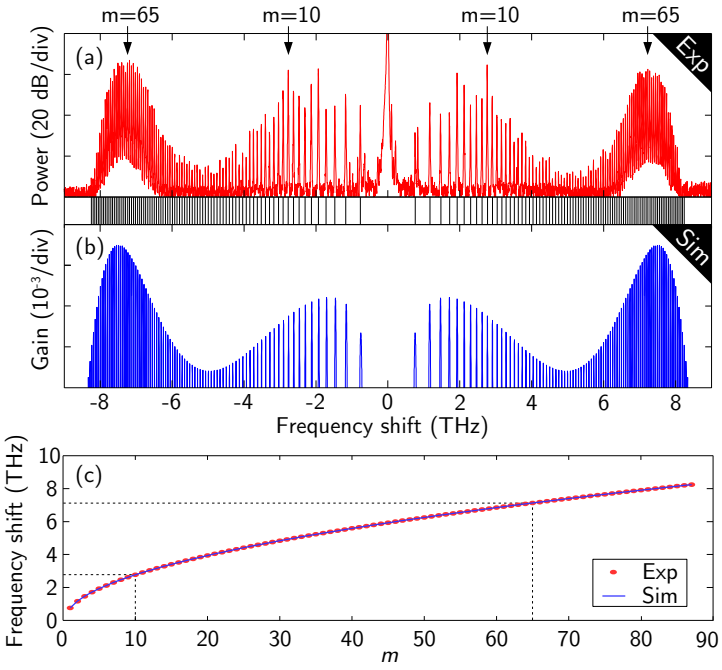

Fig. 7. (a) Experimental spectrum at the output of the cavity showing 87 pairs of sidebands symmetrically located around the pump. (b) Analytical gain spectrum obtained from Floquet analysis. (c) Positions of the sidebands as a function of the integer m for both experiments and analytics (Eq. 5). Here $\lambda_P = 1550.3\ nm$.

pump wavelength as before ($\lambda_P = 1550.3\ nm$). The plot of the spectrum is restricted to one side of the pump for the sake of clarity. The pump, which is supposed to appear at null frequency shift, has been filtered out before detection to help detecting weak parametric sidebands without saturating the detector.

It appears from this 2D color plot that the system goes through a transient regime, which lasts nearly 800 round-trips. First, multiple sidebands appear around the round-trip 150 and we can identify the low frequency components (range $0-4\ THz$) and the cluster of sidebands (range $6-8\ THz$). Note that the rather large noise level of the DFT setup prevent us from revealing the weakest sidebands which are expected to appear between 4 and 6 THz (see Fig. 7(a)). After the 500-th round-trip the cluster has completely vanished and some low frequency sidebands persist until the 800-th round-trip. After that, only 4 sidebands (corresponding to $m = 1, 2, 5\ and\ 6$) "survive" and persist as long as the driving field is sustained (although we recorded this steady spectrum for more than 6000 round-trips, we reported a truncated version for the sake of clarity). Two snapshots at round-trips 1500 and 400 are plotted in Fig. 8(a) and (c), respectively.

We carried out numerical simulations of the LL model (Eq. (1)) with dispersion truncated up to the FOD term, and the results are plotted in Fig. 8(d-f) for comparison. The main features are well reproduced and a stable spectrum arises after a transitory regime of a few hundred round-trips. These results constitute a clear evidence of a competition scenario driven by the parametric gain.

A perfect quantitative agreement is not achieved in Fig. 8 because MI is a noise driven process where the random initial conditions play a critical role both in experiments and simulations [25, 26]. We illustrate this fact in Fig. 9 by plotting side-by-side the output spectrum of three different realizations of both experiments (Fig. 9(a)) and simulations (Fig. 9(b)) after 400 round-

Optics EXPRESS

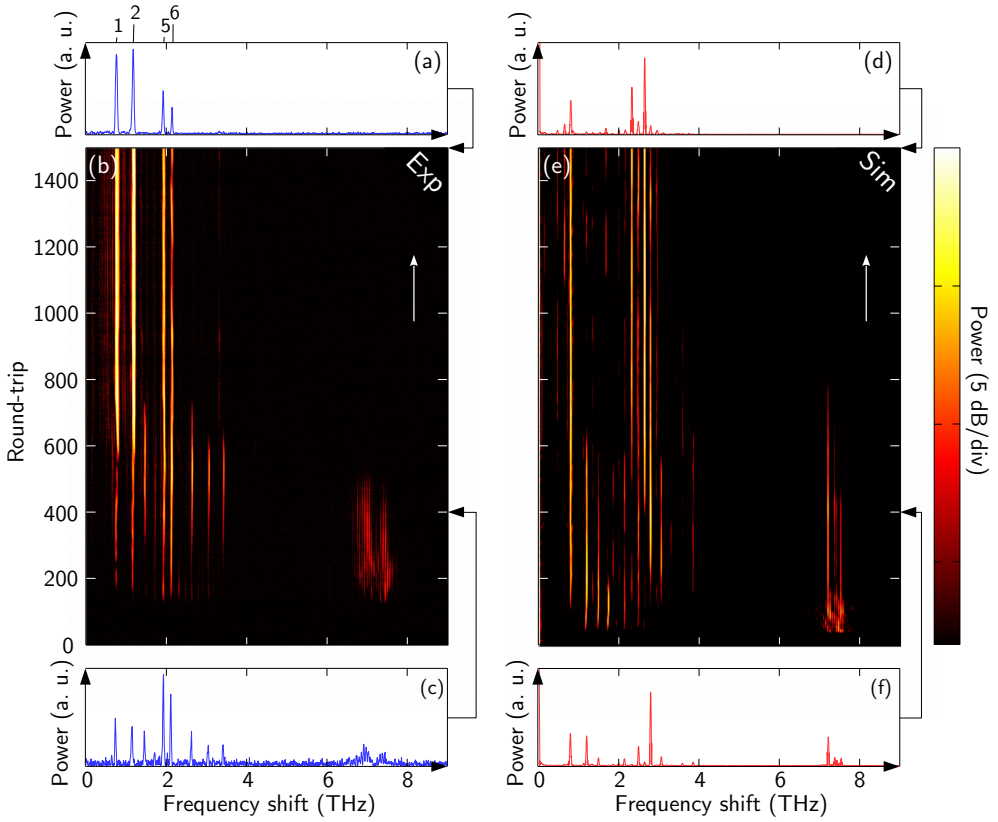

Fig. 8. (b) 2D color logarithmic plot of the real time evolution of the spectrum for the first 1500 round-trips of a burst. The beginning of the burst corresponds to the round-trip 0. (a, c) Snapshots of (b) for round-trips 400 and 1500 respectively. (d-f) Corresponding numerical simulations.

trips. Those realizations only differ from each other by the random initial conditions. It clearly appears that, at this stage, of the experiment/simulation, a large variety of results can be obtained. This is further illustrated in Visualization 1, which shows the roundtrip-to-roundtrip evolution of the output spectrum during the first 400 round-trips for 40 realizations of the experiment using the short burst pumping and the DFT technique. Each realization leads to a different result.

4. Conclusion

In conclusion, we demonstrated that, under low dispersion conditions, an unprecedented large number of quasi-phase-matched frequency sidebands can appear in dispersion oscillating passive fiber-ring cavities pumped in the low dispersion regime. For the relevant case of cavities with piecewise constant parameters, we developed a theoretical model based on an extended mean-field Lugiato-Lefever model that allows us to compute the parametric gain by taking into account higher order dispersion terms. In particular, we show that the fourth order dispersion β_4 strongly affects the gain spectrum when the cavity is pumped close to a zero dispersion wavelength, and leads to high frequency clusters of sidebands. To confirm this experimentally, we built a fiber-ring cavity with a specially tailored longitudinal dispersion profile. By periodically turning on and off the driving field, we managed to record a remarkably large number of sideband pairs, up to 87, in a single spectrum, in perfect agreement with theoretical predictions. The dependence

Optics EXPRESS

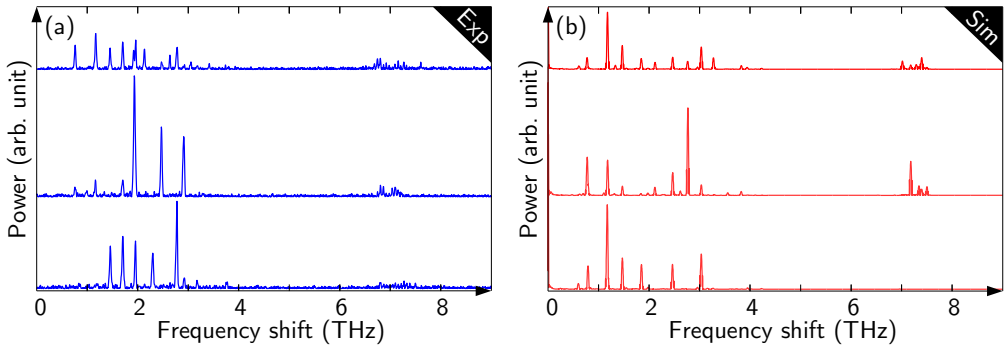

Fig. 9. Power spectrum after 400 round-trips of 3 consecutive shots: (a) experiments; (b) simulations. Only the random noise conditions differ from one shot to the other.

of the instability spectrum on the pump wavelength is also clearly observed. Finally, we proceed to the recording of the dynamical evolution of the instability spectrum disclosing the birth of the sidebands and their interactions until a stationary state is reached. These results, in agreement with numerical simulations of the mean-field model, provide an example of the dynamics of gain competition in a parametric process. Such an investigation of the real-time evolution of the system was made possible thanks to the very low free spectral range of macroscopic fiber cavities compared to microresonators. Also, this study is clearly of interest in the domain of microresonators where a similar azimuthal modulation of the cavity dispersion leads to Faraday instability which can trigger the formation of Kerr frequency combs [27].

Funding

Agence Nationale de la Recherche NoAWE (ANR-14- ACHN-0014) and TOPWAVE (ANR-13-JS04-0004) projects; LABEX CEMPI (ANR-11-LABX-0007); Equipex Flux (ANR-11-EQPX-0017); Ministry of Higher Education and Research, Nord-Pas de Calais Regional Council; European Regional Development Fund (ERDF) through the Contrat de Projets Etat-Region (CPER Photonics for Society P4S); IRCICA, USR 3380, CNRS-Univ, F-59000 Lille, France (http://www.ircica.univ-lille1.fr); PRIN (2012BFNWZ2).

Acknowledgments

We thank Laure Lago and Julie Beaucé for providing us with the fiber Bragg gratings.